Multiwall MoS$_2$ tubes as optical resonators

D. R. Kazanov,[1,a)] A. V. Poshakinskiy,[1] V. Yu. Davydov,[1] A. N. Smirnov,[1] I. A. Eliseyev,[1]
D. A. Kirilenko,[1] M. Remškar,[2] S. Fathipour,[3,b)] A. Mintairov,[1,3] A. Seabaugh,[3] B. Gil,[1,4]
and T. V. Shubina[1]

[1]Ioffe Institute, 26 Politekhnicheskaya, St. Petersburg 194021, Russia
[2]Jožef Stefan Institute, Jamova cesta 39, 1000 Ljubljana, Slovenia
[3]University of Notre Dame, Notre Dame, Indiana 46556, USA
[4]L2C, UMR 5221 CNRS-Université de Montpellier, Montpellier F-34095, France

We study the optical properties of MoS$_2$ nanotubes (NTs) with walls comprising dozens of monolayers. We reveal strong peaks in micro-photoluminescence (μ-PL) spectra when detecting the light polarized along the NT axis. We develop a model describing the optical properties of the nanotubes acting as optical resonators which support the quantization of whispering gallery modes inside the NT wall. The experimental observation of the resonances in μ-PL allows one to use them as a contactless method of the estimation of the wall width. Our findings open a way to use such NTs as polarization-sensitive components of nanophotonic devices. *Published by AIP Publishing.*
https://doi.org/10.1063/1.5047792

Optical microcavities of different materials and diverse forms such as planar Bragg resonators with Fabry-Pérot modes and toroidal resonators or microspheres with whispering gallery modes (WGMs) have been proposed for a wide range of potential applications.[1] In particular, the tubular microcavities have attracted much attention due to their interesting properties, such as light polarization and three dimensional mode confinement.[2] Emerging studies of micro- and nanotubes as optical resonators show that they can support the WGMs selectively enhancing light. However, the studies concerned mostly those that were made from thin films or membranes rolled up into tubes. For instance, rolled-up SiO/SiO$_2$ microcavities show resonant modes with the polarization parallel to the tube axis.[3] The on-chip nanotubes (NTs) with InGaN/GaN quantum wells demonstrated lasing controlled by the WGM resonances.[4]

After discovery of the famous carbon nanotubes (NTs),[5] a large variety of inorganic NTs have appeared.[6,7] They can be divided into two groups depending on the types of bonds between constituent monolayers within a NT wall that are either covalent/ionic bonds, e.g., in ZnO and GaN NTs[8,9] or van der Waals (vdW) forces. The vdW NTs were made of transition metal dichalcogenides (TMDCs) such as MoS$_2$, WS$_2$, WSe$_2$, and some other materials including BN. All of them have a form of a hollow cylinder with a diameter varying from nanometers to several micrometers and length approaching several millimeters. Their walls may comprise a single monolayer or multiple monolayers.[10–13] The TMDC NTs attract attention due to the unique properties of parent 2D materials, whose band structure strongly depends on the number of layers.[14] In the monolayer limit, they have an optical gap around 1.8 eV and exhibit exciton resonances with strong oscillator strength.[15]

The band structure and optical properties of single-wall TMDC NTs were studied theoretically using calculations based on the density functional theory.[16] It was also predicted that the electronic properties of multiwall NTs of MoS$_2$ should tend to those of the bulk.[17] In addition, it was shown that the band structure, density of states, and vibrational characteristics of NTs depend on strain and folding.[18–21] Currently, the TMDC NTs are becoming promising for future applications in nanoelectronics and optoelectronics. In particular, it was demonstrated that TMDC multiwall NTs and nanoribbons can be used to create such nanodevices as field-effect transistors with high current densities, and it was also shown that NTs could be used as high-performance photodetectors.[22–24] The optical properties of NTs made of 2D vdW materials slipped away from the focus of previous research. The luminescence from TMDC nanoscrolls has been only recently reported.[25]

In this paper, we show TMDC NT optical resonators with a strong selection of modes. To elucidate the optical properties of NTs near the frequency of the direct A-exciton transitions, we performed micro-photoluminescence (μ-PL) spectroscopy measurements in the range of 1.6–2.0 eV. They have shown the enhancement of emission by the strong peaks which are polarized along the tube axis x. We demonstrate that this selective enhancement is related to the WGM circulating inside the wall of NT.

The studied NTs were grown by chemical transport reaction, using iodine as a transport agent, with a very slow rate from the vapor phase that enables us to produce NTs with an extremely low density of structural defects.[11,26] We have chosen MoS$_2$ NTs which possess brighter emission as compared with WS$_2$ ones, where the lowest excitonic state is dark (see Ref. 27 and references therein), although similar resonant features were observed in these tubes as well. The studied NTs have a form of the hollow cylinders with outer radius $\approx$0.5–1 μm and the wall width $\approx$20–100 nm. The NT cross-sections can be almost ideally round.[12] The typical side view of a MoS$_2$ NT is depicted in Fig. 1(b). μ-PL measurements were performed on a Horiba Jobin-Yvon T64000 spectrometer equipped with a confocal microscope, a silicon

a)kazanovdr@beam.ioffe.ru
b)Present address: Department of Materials Science and Engineering, University of California, Berkeley, California 94720, USA.
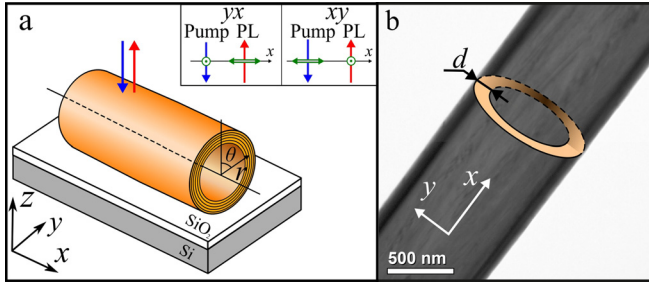
FIG. 1. (a) A sketch of a multiwall MoS$_2$ nanotube on the SiO$_2$/Si substrate. The studied NT has the outer radius 1 μm and 45-monolayer wall determined from the fitting procedure. Blue and red lines depict the pump and PL of NT, respectively. The inset shows two different configurations of the μ-PL experiment where green arrows indicate the light polarization. (b) A typical side-view transmission microscopy image of a MoS$_2$ NT. We depict a cross-section of the NT as a bright ring. The number of monolayers inside the NT wall can be estimated by dividing d/L, where L is the interlayer distance in MoS$_2$ stack ($\sim$0.6 nm).

CCD cooled by liquid nitrogen, and a 600 lines/mm grating. A Nd:YAG-laser line at a wavelength of 532 nm ($\hbar\omega_{exc} = 2.33$ eV) was used for cw excitation. The measurements in the temperature range from 80 to 250 K were carried out in a temperature controlled microscope stage Linkam THMS600. A large working distance lens [Mitutoyo 100 × NIR (NA = 0.50)] with a spot size of $\approx 2\,\mu$m on a sample was used to measure PL from a single NT.

Two different experimental configurations were used in the μ-PL studies [see the inset in Fig. 1(a)]. In the yx-configuration, excitation was performed with the light polarization (green arrows) perpendicular to the tube x-axis (along y) and the light polarized along the x-axis (TM-polarized) was detected. In the xy-configuration, the excitation was x-polarized while y-polarized PL was detected.

The experimental μ-PL spectra recorded in these two configurations at 80 K are shown in Fig. 2. PL spectra manifest peaks at 1.83 eV and 1.92 eV related to A- and B-excitons, respectively, close to those in planar MoS$_2$ layers.[14] Both PL spectra exhibit A-exciton emission with a long tail which reveals a sequence of peaks in the yx-configuration (red line), while in the xy-configuration (blue line), these peaks are suppressed. The nature of peaks in the yx-configuration seems to be due to the WGMs inside the NT wall. They provide the enhancement of PL intensity which is usually rather weak in the planar multilayer structures due to the indirect nature of the bandgap in bulk.[14] The quality factor of the modes, defined as $Q = E/\Delta E$, where E is the energy and ΔE is the FWHM of the resonant peak in spectra, is around 90. Also, the free spectral range (FSR), i.e., the energy splitting between modes, for x-polarized modes varies from $\sim$50 to 20 meV. The decrease in the FSR with the increase in energy is due to the increase in the refractive index of the material near the A-exciton.[28] Similar behavior occurred in other semiconductor resonators.[29,30]

The temperature dependent measurements in the yx-configuration (Fig. 3) showed that resonant modes are red-shifted when temperature increases. This is caused by a shrink of the bandgap of the material and, thus, the shift of all resonances. Such behavior is typical for the TMDC material and was previously observed in temperature dependent PL studies.[31,32] Besides, the total PL intensity decreases with
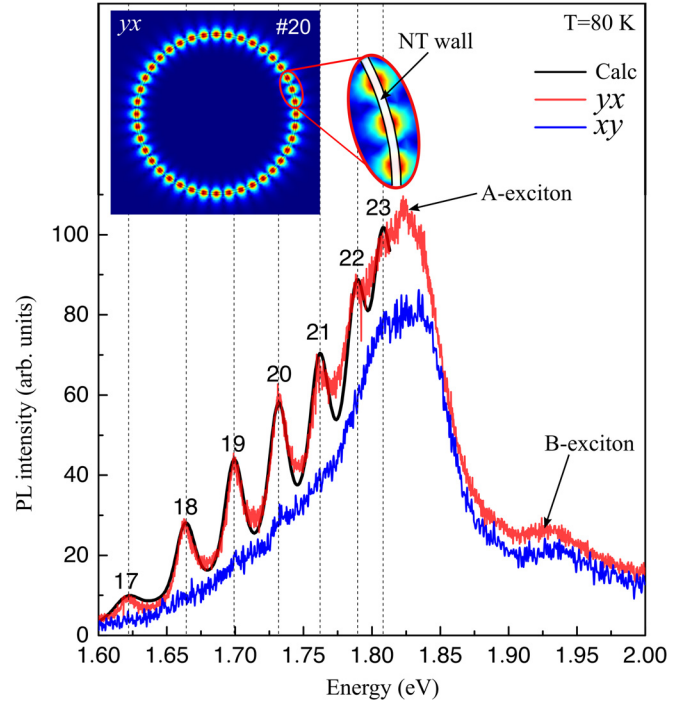

FIG. 2. Experimental spectra of μ-PL in the yx (red line) and xy (blue line) polarization configurations with 1 mW excitation power. The spectrum in the yx configuration exhibits peaks related to the optical modes. The calculated spectrum for PL in the same configuration is shown by the black line. The angular number of the modes is indicated above the corresponding peak. The inset represents the electric field distribution for x-polarized WGM with angular number $m = 20$.

temperature due to the increase in the non-radiative exciton decay rate. However, resonant peculiarities are still present in the high-temperature spectra. It means that such NTs can be used as polarization sensitive-devices or filters even at room temperatures.

To confirm the origin of the PL peaks in the yx-configuration and to explain their suppression in the xy configuration, we performed the theoretical modeling of the PL spectra of the TMDC NTs. Due to the cylindrical symmetry of the system, we describe the electromagnetic field in cylindrical coordinates (x, r, θ), where $\theta = 0°$ is related to the
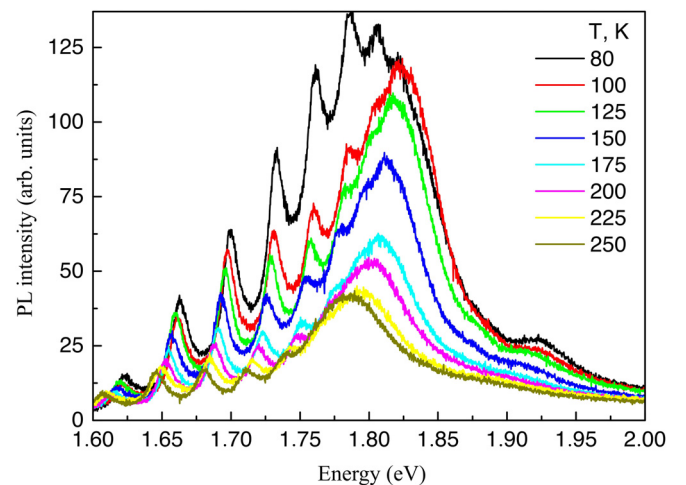

FIG. 3. Temperature dependent μ-PL spectra in the yx configuration for temperatures varying from 80 K to 250 K.

direction of the incident laser beam. The PL intensity from the NT volume with coordinates (r, θ) is proportional to the squared amplitude of the incident electric field at that point. Thus, to calculate PL spectra, we should find the excitation power inside the NT walls. The electric field inside the wall of the NT can be found by solving a scattering problem of normally incident light on NT, as described in the supplementary material. The components of the electric field from the incident laser beam that lie in the plane of the NT wall generate excitons with spatial distribution $P^{(y,x)}(r, \theta, \omega_{\text{exc}})$ $\sim |E_x^{(y,x)}(r, \theta, \omega_{\text{exc}})|^2 + |E_\theta^{(y,x)}(r, \theta, \omega_{\text{exc}})|^2$, where $\boldsymbol{E}^{(x)}$ is the electric field inside the NT under x-polarized excitation with frequency ω_{exc}, and $\boldsymbol{E}^{(y)}$ is the electric field in the case of y-polarized excitation, see Eq. (S7) from the supplementary material. The exciton generation is followed by rapid energy relaxation with the conservation of real space distribution and loss of polarization. The subsequent reemission of photons yields the PL which is modulated by the resonator modes.

In order to calculate the PL spectra for any polarization of the detected light, we use the Lorentz reciprocity theorem. We replace the problem of light emission from the system in a certain direction by the problem of scattering of the plane wave incident from this direction.[33,34] The PL spectra for two experimental configurations are then given by

$$\text{PL}_{yx}(\omega) = \int\int |E_x^{(x)}(r, \theta; \omega)|^2 P^{(y)}(r, \theta, \omega_{\text{exc}})\, dr\, d\theta, \quad (1)$$

$$\text{PL}_{xy}(\omega) = \int\int |E_\theta^{(y)}(r, \theta; \omega)|^2 P^{(x)}(r, \theta, \omega_{\text{exc}})\, dr\, d\theta. \quad (2)$$

Integration is performed over the NT cross-section. The $E^{(x,y)}(r, \theta, \omega)$ fields have the same form as the pump field Eq. (S7), but they oscillate at the frequency of detection ω.

To simulate the real PL spectra, one should know not only the electric field distribution that generates excitons in the wall in the real space but also mandatory to know the energy distribution of generated excitons. As we see in Fig. 2, blue line, the y-polarized PL spectrum exhibits negligible resonant peaks; thus, we can use this spectrum as a description of such distribution. We also account for the deviation of the number of monolayers in the NT wall. We relate both the widths and heights of the experimental peaks in terms of a distribution of the wall width of 1 monolayer. The frequency dependent refractive index was taken into account. Its variation was expressed via the combination of the background part and the exciton contribution taking into account the experimental spectra, reported in Ref. 28.

The observed WGMs have zero wave vector along the NT axis while they vary in the azimuthal direction as $e^{im\phi}$, where m is the azimuthal angular number. The electric field of the modes can be either parallel or perpendicular to nanotube axis x. The x-polarized WGMs with the energies below the A-exciton in MoS_2 are characterized by m ranging from 17 to 23. The peak amplitudes vary with m non-monotonously due to the competition of two factors. First, the mode quality factor increases with the azimuthal angular number due to increasing mode confinement inside the NT

wall. After a certain energy, which appears to correspond to $m = 20$ for the studied NT, this effect is diminished by the decrease in the mode quality factor due to the increasing imaginary part of the refractive index as the energy of the direct exciton is approached. The electric field distribution of the mode with angular number $m = 20$ is shown in the inset of Fig. 2. Modes above 1.8 eV are strongly suppressed due to the high background absorption.

The modeling of y-polarized modes has shown that they also can be found in this spectral range, but their angular numbers are lower and vary around 5. In cylindrical cavities, both the radiative decay and, therefore, the WGM Q-factor strongly depend on the azimuthal number. The larger the m is the larger is the Q-factor.[35] This effect is even more pronounced in the tubular geometry, where confinement of the modes in the tube wall is even stronger. Because of that, the y-polarized modes with the small angular numbers are not revealed in the PL spectra. For the measured outer radius 1 μm, taking into account the frequency dependent refractive index of MoS_2 and the 1-monolayer fluctuation of the wall width, we obtain a perfect agreement between experimental peak positions, widths, and amplitudes and calculated ones, assuming the number of monolayers $N = 45$ (black line in Fig. 2). Thus, such fitting of experimental spectra, taking into account the inaccuracy in the measurement of the tube diameter and possible deviation of the tube shape from a perfect cylinder and the error in the determination of the number of monolayers in the wall estimated as $\pm 5\%$, can be used as a highly accurate contactless method of NT characterization.

The modeled PL spectra in parallel polarization configurations xx and yy (not shown) exhibit almost the same behavior as in yx and xy configurations, respectively. The peaks in the xx configuration are located at the same frequencies as in the yx configuration, but their amplitudes change due to the difference in the spatial exciton distributions inside the NT wall under x- and y-polarized excitation. In the yy configuration, the resonances are not revealed, similar to the xy configuration. When the linear analyzer polarizer is rotated from the yx to yy configuration, the peaks decay as a cosine function.

For a deeper insight into the impact of the tube sizes on the optical modes, we calculated the dependencies of the mode energies with the wall width (number of monolayers) and tube radius. Figure 4 (top) shows the dependence of the x-polarized mode energies on the outer NT radius (black lines) for the fixed number of monolayers in the wall $N = 45$ and on the number of monolayers (blue lines) for fixed outer radius 1 μm. The modes with angular number $m = 10, 15, 20$, and 25 that have energies near the A-exciton are shown. Alteration of the radius influences the energy of the modes stronger than that of the monolayer number. Further, the smaller the radius is, the smaller is the mode angular number for the same mode energy; thus, the Q-factor of such a mode is lower and the light weakly interacts with this mode.

Figure 4 (bottom) demonstrates the transition from the hollow cylinder to the full one. Namely, it shows the dependence of the x-polarized mode energies with the number of monolayers in the wall. For the constant outer radius, the increase in the wall width corresponds to the decrease in the inner radius up to the formation of the full cylinder. When
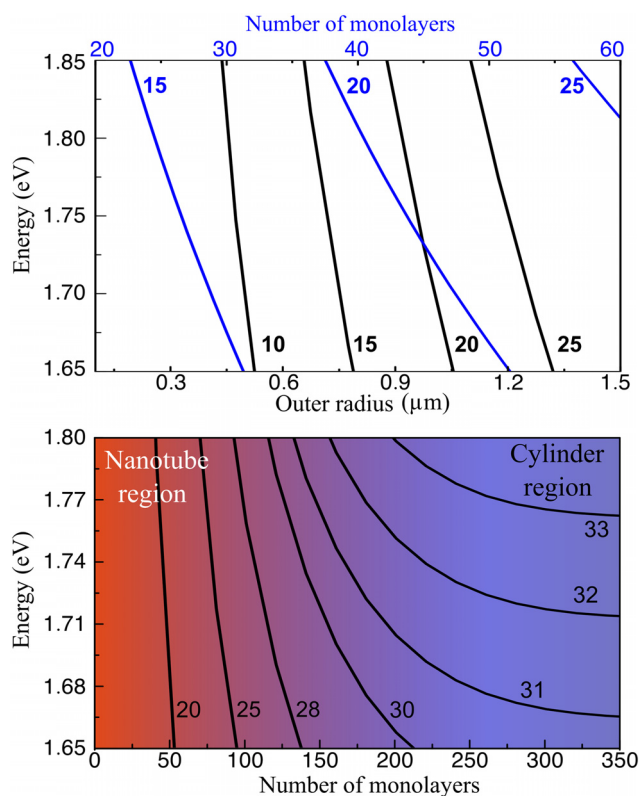
FIG. 4. (Top) Dependence of the *x*-polarized mode energies on the outer radius of the NT varying from 0.1 to 1.5 μm for the fixed number of monolayers in the wall $N = 45$ (black lines) and on the number of monolayers N varying from 20 to 60 for the fixed outer radius 1 μm (blue lines). (Bottom) Mode energies as a function of the number of monolayers varying from 1 to 350 for NT with the fixed outer radius 1 μm. Red region—light is confined inside the NT wall. Blue region—WGM is localized near the outer radius of almost full cylinder.

the NT wall width is thin (red area), there is a strong dependence of the mode energy on the number of monolayers. This is because the light is confined within the NT wall. The thinner is the wall the higher is the energy of the supported mode. With the increase in the monolayer number, the transition to a full cylinder region takes place (blue area). In this case, the WGM is localized in the vicinity of the outer NT radius and the eigenfrequencies become almost independent of the wall width and coincide with those for the full cylinder with the same external radius. The difference between the NT and the cylinder is negligible when the wall width is larger than about 20% of the outer radius.

To summarize, we have shown that the PL spectra of multiwall TMDC NTs comprise strong peaks linearly polarized along the NT axis. We modeled the μ-PL spectra of NTs for two orthogonal experimental configurations. The perfect agreement with the experimental μ-PL spectra has been obtained taking into account the inhomogeneity of NT parameters and the frequency dependence of the refractive index. We explained the difference between *x*-polarized and *y*-polarized PL spectra by the difference in angular momentum numbers of the corresponding modes in the energy region below the A-exciton. We demonstrate that the observed WGMs are confined within the NT wall, between its inner and outer surface. We propose that fitting of the PL spectra modulated by the optical modes can be used as a unique and noninvasive way to estimate the NT wall. The

pronounced PL peaks exist up to room temperature which opens the way to use the TMDC NTs as polarization-sensitive devices.

See supplementary material for the description of the light scattering problem on the NTs.

[1]K. J. Vahala, "Optical microcavities," Nature **424**, 839–846 (2003).
[2]J. Wang, T. Zhan, G. Huang, P. K. Chu, and Y. Mei, "Optical microcavities with tubular geometry: Properties and applications," Laser Photonics Rev. **8**, 521 (2014).
[3]G. S. Huang, S. Kiravittaya, V. A. Bolanos Quinones, F. Ding, M. Benyoucef, A. Rastelli, Y. F. Mei, and O. G. Schmidt, "Optical properties of rolled-up tubular microcavities from shaped nanomembranes," Appl. Phys. Lett. **94**, 141901 (2009).
[4]Y. Li, L. Feng, X. Su, Q. Li, F. Yun, G. Yuan, and J. Han, "Whispering gallery mode lasing from InGaN/GaN quantum well microtube," Opt. Express **25**, 18072 (2017).
[5]S. Iijima, "Helical microtubules of graphitic carbon," Nature **354**, 56 (1991).
[6]C. N. R. Rao and M. Nath, "Inorganic nanotubes," Dalton Trans. **1**, 1–24 (2003).
[7]R. Tenne, L. Margulis, M. Genut, and G. Hodes, "Polyhedral and cylindrical structures of tungsten disulphide," Nature **360**, 444 (1992).
[8]Y. J. Xing, Z. H. Xi, Z. Q. Xue, X. D. Zhang, J. H. Song, R. M. Wang, J. Xu, Y. Song, S. L. Zhang, and D. P. Yua, "Optical properties of the ZnO nanotubes synthesized via vapor phase growth," Appl. Phys. Lett. **83**, 1689 (2003).
[9]J. Goldberger, R. He, Y. Zhang, S. Lee, H. Yan, H.-J. Choi, and P. Yang, "Single-crystal gallium nitride nanotubes," Nature **422**, 599 (2003).
[10]N. G. Chopra, R. J. Luyken, K. Cherrey, V. H. Crespi, M. L. Cohen, S. G. Louie, and A. Zettl, "Boron nitride nanotubes," Science **269**, 966 (1995).
[11]M. Remškar, Z. Skraba, F. Cléton, R. Sanjinés, and F. Lévy, "MoS$_2$ as microtubes," Appl. Phys. Lett. **69**, 351 (1996).
[12]M. Remškar, "Inorganic nanotubes," Adv. Mater. **16**, 1497 (2004).
[13]M. Remškar, A. Mrzel, Z. Skraba, A. Jesih, M. Ceh, J. Demšÿar, P. Stadelmann, F. Lévy, and D. Mihailovic, "Self-assembly of subnanometer-diameter single-wall MoS$_2$," Science **292**, 479 (2001).
[14]K. F. Mak, C. Lee, J. Hone, J. Shan, and T. F. Heinz, "Atomically thin MoS$_2$: A new direct-gap semiconductor," Phys. Rev. Lett. **105**, 136805 (2010).
[15]J. Xiao, M. Zhao, Y. Wang, and X. Zhang, "Excitons in atomically thin 2D semiconductors and their applications," Nanophotonics **6**, 1309 (2017).
[16]G. Seifert, H. Terrones, M. Terrones, G. Jungnickel, and T. Frauenheim, "Structure and electronic properties of MoS$_2$ nanotubes," Phys. Rev. Lett. **85**, 146 (2000).
[17]G. Seifert, H. Terrones, M. Terrones, G. Jungnickel, and T. Frauenheim, "On the electronic structure of WS$_2$ nanotubes," Solid State Commun. **114**, 245 (2000).
[18]M. Viršek, A. Jesih, I. Milošević, M. Damnjanović, and M. Remškar, "Raman scattering of the MoS$_2$ and WS$_2$ single nanotubes," Surf. Sci. **601**, 2868 (2007).
[19]M. Viršek, A. Krause, A. Kolitsch, and M. Remškar, "Raman characterization of MoS$_2$ microtube," Phys. Status Solidi B **246**, 11 (2009).
[20]N. Zibouche, M. Ghorbani-Asl, T. Heine, and A. Kuc, "Electromechanical properties of small transition-metal dichalcogenide nanotubes," Inorganics **2**, 155 (2014).
[21]F. Wang, I. A. Kinloch, D. Wolverson, R. Tenne, A. Zak, E. O'Connell, U. Bangert, and R. J. Young, "Strain-induced phonon shifts in tungsten disulfide nanoplatelets and nanotubes," 2D Mat. **4**, 015007 (2017).
[22]M. Strojnik, A. Kovic, A. Mrzel, J. Buh, J. Strle, and D. Mihailovic, "MoS$_2$ nanotube field effect transistors," AIP Adv. **4**, 097114 (2014).
[23]S. Fathipour, M. Remškar, A. Varlec, A. Ajoy, R. Yan, S. Vishwanath, S. Rouvimov, W. S. Hwang, H. G. Xing, D. Jena, and A. Seabaugh, "Synthesized multiwall MoS$_2$ nanotube and nanoribbon field-effect transistors," App. Phys. Lett. **106**, 022114 (2015).

[24]C. Zhang, S. Wang, L. Yang, Y. Liu, T. Xu, Z. Ning, A. Zak, Z. Zhang, R. Tenne, and Q. Chen, "High-performance photodetectors for visible and near-infrared lights based on individual WS_2 nanotubes," Appl. Phys. Lett. **100**, 243101 (2012).

[25]X. Cui, Z. Kong, E. Gao, D. Huang, Y. Hao, H. Shen, C.-A. Di, Z. Xu, J. Zheng, and D. Zhu, "Rolling up transition metal dichalcogenide nanoscrolls via one drop of ethanol," Nat. Commun. **9**, 1301 (2018).

[26]M. Remškar, Z. Skraba, M. Regula, C. Ballif, R. Sanjines, and F. Levy, "New crystal structures of WS_2: microtubes, ribbons, and ropes," Adv. Mater. **10**, 246 (1998).

[27]E. Malic, M. Selig, M. Feierabend, S. Brem, D. Christiansen, F. Wendler, A. Knorr, and G. Berghäuser, "Dark excitons in transition metal dichalcogenides," Phys. Rev. Mater. **2**, 014002 (2018).

[28]H. Zhang, Y. Ma, Y. Wan, X. Rong, Z. Xie, W. Wang, and L. Dai, "Measuring the refractive index of highly crystalline monolayer MoS_2 with high confidence," Sci. Rep. **5**, 8440 (2015).

[29]T. V. Shubina, G. Pozina, V. N. Jmerik, V. Y. Davydov, C. Hemmingsson, A. V. Andrianov, D. R. Kazanov, and S. V. Ivanov, "III-nitride tunable cup-cavities supporting quasi whispering gallery modes from ultraviolet to infrared," Sci. Rep. **5**, 17970 (2015).

[30]Y. Mi, Z. Zhang, L. Zhao, S. Zhang, J. Chen, Q. Ji, J. Shi, X. Zhou, R. Wang, J. Shi, W. Du, Z. Wu, X. Qiu, Q. Zhang, Y. Zhang, and X. Liu, "Tuning excitonic properties of monolayer MoS_2 with microsphere cavity by high-throughput chemical vapor deposition method," Small **13**, 1701694 (2017).

[31]T. Korn, S. Heydrich, M. Hirmer, J. Schmutzler, and C. Schüller, "Low-temperature photocarrier dynamics in monolayer MoS_2," Appl. Phys. Lett. **99**, 102109 (2011).

[32]J. S. Ross, S. Wu, H. Yu, N. J. Ghimire, A. M. Jones, G. Aivazian, J. Yan, D. G. Mandrus, D. Xiao, W. Yao, and X. Xu, "Electrical control of neutral and charged excitons in a monolayer semiconductor," Nat. Commun. **4**, 1474 (2013).

[33]N. A. Gippius, S. G. Tikhodeev, and T. Ishihara, "Optical properties of photonic crystal slabs with an asymmetrical unit cell," Phys. Rev. B **72**, 045138 (2005).

[34]M. Iwanaga, A. S. Vengurlekarand, T. Hatano, and T. Ishihara, "Reciprocal transmittances and reflectances: An elementary proof," Amer. J. Phys. **75**, 899 (2007).

[35]M. A. Kaliteevski, S. Brand, R. A. Abram, A. Kavokin, and L. S. Dang, "Whispering gallery polaritons in cylindrical cavities," Phys. Rev. B **75**, 233309 (2007).